

# Energetic Ions Downtail of the Reconnection Site

Joachim Birn<sup>1,2</sup>, Michael Hesse<sup>3</sup>, Andrei Runov<sup>4</sup>, Drew Turner<sup>5</sup>, Ian Cohen<sup>5</sup>,  
and James A. Slavin<sup>6</sup>

<sup>1</sup>Space Science Institute, Boulder, CO, USA

<sup>2</sup>Guest Scientist, Los Alamos National Laboratory, Los Alamos, NM, USA

<sup>3</sup>NASA Ames Research Center, Moffett Field, CA, USA

<sup>4</sup>Department of Earth, Planetary, and Space Sciences, University of California, Los Angeles, CA, USA

<sup>5</sup>Space Exploration Sector, The Johns Hopkins Applied Physics Laboratory, Laurel, MD, USA

<sup>6</sup>Dept. Climate and Space Sciences and Engineering, U. Michigan, Ann Arbor, MI, USA

## Key Points:

- Energetic ion fluxes form tailward beams surrounding the plasmoid but multiple separate branches near the equatorial plane.
- Boundary beams are primarily accelerated near x-line, equatorial acceleration occurs anywhere across tailward propagating plasmoid.
- Origins of accelerated ions are primarily in the dawnward central plasma sheet.

---

Corresponding author: Joachim Birn, [jbirn@spacescience.org](mailto:jbirn@spacescience.org)

This is the author manuscript accepted for publication and has undergone full peer review but has not been through the copyediting, typesetting, pagination and proofreading process, which may lead to differences between this version and the [Version of Record](#). Please cite this article as [doi: 10.1029/2021JA029892](https://doi.org/10.1029/2021JA029892).

This article is protected by copyright. All rights reserved.

## Abstract

Using combined MHD/test particle simulations, we explore characteristics of ion (proton) acceleration tailward of a near-Earth reconnection site. We present spatial distributions and explore acceleration mechanisms and sources of accelerated ions. Acceleration is due primarily due simple crossings of the enhanced electric field near the x-line or in the departing plasmoid. The energetic particle distributions show the expected energy dispersed tailward streaming at the plasma sheet boundary, while equatorial distributions are more complicated, resulting from different acceleration sites within the moving plasmoid. Sources are mostly inside the central plasma sheet downward of the plasmoid.

## 1 Introduction

The Earth's magnetotail plays a prominent role in the dynamics of the magnetosphere, as a site of temporary energy storage and sudden release, involving magnetic reconnection and causing ground disturbances and auroral displays. Its different regions are here denoted as follows:

“Near tail” denotes the region earthward of about 25 to 30 Earth radii ( $R_E$ ) down to geosynchronous orbits, which includes the region where, according to standard substorm models, a new reconnection site forms, governing substorm and other activity. This region has been explored most recently by the satellite missions Cluster (Escoubet et al., 2001), “Time History of Events and Macroscale Interactions during Substorms” (THEMIS) (Angelopoulos, 2008), and “Magnetospheric Multiscale” (MMS) (Burch et al., 2016). Earlier observations by “Orbiting Geophysical Observatory” (OGO) and Vela satellites in this region, together with ground magnetic observations, have laid the basis for the now widely accepted “Near-Earth Neutral Line” model of substorms (McPherron et al., 1973; Hones Jr., 1977; Baker et al., 1996), which states that substorm features are closely related to the formation of reconnection in this region, associated with earthward and tailward plasma flows, a collapse (“dipolarization”) of the inner tail, and the severance of a portion of the plasma sheet and its ejection as a plasmoid. Essential elements of this model had already been suggested by Atkinson (1966, 1967).

“Far tail,” “deep tail,” or “distant tail” denotes the region beyond the distance of the Moon, which has been explored until recently only by two satellite missions, “International Sun-Earth Explorer”-3 (ISEE-3) (Bame et al., 1983; Slavin et al., 1983; Hones Jr., Baker, et al., 1984; Zwickl et al., 1984; Tsurutani et al., 1984; Tsurutani & von Rosenvinge, 1984) and Geotail (Nishida, 1994; Kokubun et al., 1994; Mukai et al., 1994; Machida et al., 1994). This region typically includes a “distant neutral line” (Hones Jr., 1977; Baker et al., 1984), which is considered to terminate the region of closed field lines, which are connected to Earth at both ends during quiet times, and may also be the site of reconnection.

The region in between is termed here “mid tail.” It covers the region of the departing plasmoids (e.g., Hones Jr., 1977; Galeev, 1979), potential earthward flows from the distant neutral line (e.g., Kiehas et al., 2018), but may also be the site of, presumably reconnection related, local activity (Sergeev et al., 1996). This region is the main region of interest in the present investigation, although our results may be pertinent also for the more distant magnetotail. It was first explored by Explorer satellites (also labeled “International Monitoring Platform,” IMP) with Explorers 33 and 35 being the first satellites to establish the tail magnetic geometry out to and beyond the distance of the Moon (Ness et al., 1967b, 1967a; Behannon, 1968; Mihalov & Sonett, 1968). Mihalov et al. (1968) established the persistence of a magnetic field component normal to the neutral sheet, taking the occasional southward turning as evidence of reconnection earthward from the satellites. Armstrong and Krimigis (1968) and Fennell (1970) reported Explorer 33 and 35 observations of proton bursts with energies above 0.31 MeV in the tail region out to

67 and beyond the Moon's distance. These flows were preferentially, but not always, anti-  
68 earthward, mostly aligned with the magnetic field, and closely related to auroral bay ac-  
69 tivity.

70 Based on IMP-7 observations at  $\sim 35R_E$  distance, Sarris, Krimigis, and Armstrong  
71 (1976) identified proton bursts with energies above 0.29 MeV (and electron bursts with  
72  $E_e \geq 0.22$  MeV) in the plasma sheet (as well as in the boundary layer and the mag-  
73 netosheath). The bursts showed anisotropies both toward and away from Earth together  
74 with a significant dawn-to-dusk component and also an association with magnetic ac-  
75 tivity. Sarris, Krimigis, Iijima, et al. (1976) reported IMP-6 and IMP-7 observations of  
76 proton bursts near  $x_{SM} \approx -32R_E$  in association with a substorm, indicating a nearby  
77 source with a location first tailward, then earthward of the satellites.

78 On the basis of ISEE-3 data, Scholer et al. (1983) found that suprathermal pro-  
79 tons with energies above  $\sim 35$  keV are a persistent feature of the distant tail and Daly  
80 et al. (1984), without distinguishing between quiet and disturbed times, found an almost  
81 equal occurrence of tailward and earthward streaming energetic ions above 35 keV at dis-  
82 tances below  $\sim 100 R_E$  but a strong preponderance of tailward streaming beyond. Cowley  
83 et al. (1984) also reported energetic ions streaming mainly tailward, particularly in bound-  
84 ary layers of the distant plasma sheet. ISEE-3 observations in the far tail (Hones Jr., Baker,  
85 et al., 1984; Scholer, Gloeckler, Klecker, et al., 1984; Scholer, Gloeckler, Hovestadt, et  
86 al., 1984; Richardson & Cowley, 1985; Richardson et al., 1987) provided a detailed de-  
87 scription of energetic particle properties associated with plasmoids, showing energy dis-  
88 persed energetic ions streaming tailward along the magnetic field at the boundary of tail-  
89 ward moving plasmoids, while the interior was characterized by more broadly distributed,  
90 apparently tailward convecting populations. (The ion plasma instrument on ISEE-3 was  
91 not functioning during the far tail mission.)

92 The conclusions from ISEE-3 observations were confirmed and expanded by ion plasma  
93 observations of Geotail (e.g., Nagai et al., 1994; Ieda et al., 1998; Håland et al., 1999;  
94 Machida et al., 2000) and the, lunar orbiting, Acceleration, Reconnection, Turbulence,  
95 and Electrodynamics of Moons Interaction with the Sun (ARTEMIS) spacecraft (Angelopoulos,  
96 2011). Runov et al. (2018) conducted a statistical analysis of tailward reconnection out-  
97 flows captured by the ARTEMIS probes. They showed that typical ion energy spectra  
98 obtained in the outflows are characterized by increased fluxes at energies above 10 keV  
99 compared to the ion spectra in the background plasma sheet, while the spectral shape  
100 was non-Maxwellian with a pronounced high energy tail. Grigorenko et al. (2019) stud-  
101 ied ion and electron beams observed by the ARTEMIS probes near the plasma sheet bound-  
102 ary layer. They found no significant differences in characteristics between earthward and  
103 tailward ion beams, nor between beams observed on open or closed field lines. However,  
104 tailward ion beams tended to be shorter and more closely related to high absolute val-  
105 ues of the AL index, that is, geomagnetic activity.

106 A few attempts have been made to model the acceleration and fluxes of energetic  
107 ions in the mid and distant tail. The large extent of the region of interest from the near-  
108 Earth reconnection site to the distance of the Moon and beyond obviously does not per-  
109 mit a fully self-consistent particle simulation. Zeleny et al. (1984) and Zelenyi et al. (1990)  
110 used a largely analytic approach to address the ion and electron acceleration in the vicin-  
111 ity of an x-line, based on the explosive growth of a tearing mode (Galeev, 1979) in a two-  
112 dimensional configuration, neglecting variations in the cross-tail ( $y$ ) direction. They demon-  
113 strated efficient acceleration from the inductive electric field and the formation of power-  
114 law high-energy distributions.

115 Investigations that have taken the large-scale tail structure into account have used  
116 a combination of MHD simulation with test particle tracing in the fields of this simu-  
117 lation. In particular, Scholer and Jamitzky (1987, 1989) used a two-dimensional MHD  
118 simulation of near tail reconnection and plasmoid ejection to study the acceleration of

119 protons in the electric and magnetic fields of the simulation. In their simulations, en-  
 120 ergized protons originated from the lobes at various distances in  $x$  and were accelerated  
 121 in the vicinity of the near-Earth x-line. The subsequent motion toward the distant tail  
 122 lead to strongly field-aligned fluxes close to the plasma sheet boundary with the expected  
 123 spatial dispersion of the largest energies closest to the boundary.

124 Birn et al. (2004) followed a similar approach, however, based on a three-dimensional  
 125 MHD simulation (Birn & Hesse, 1996). They focused particularly on the acceleration  
 126 of  $O^+$  ions, but included also results on  $H^+$  ions, at a single final energy of 180 keV. They  
 127 also found the resulting energetic ion fluxes concentrated close to the plasma sheet bound-  
 128 ary. However, the particles originated not only from the lobes but, to a significant amount,  
 129 from inside the plasma sheet downward of the observation site.

130 Here we use a similar procedure, based on the three-dimensional, time-dependent  
 131 fields of an MHD simulation of near-tail reconnection, flow bursts, and plasmoid ejection  
 132 (Birn et al., 2011). In contrast to the earlier MHD simulation (Birn & Hesse, 1996),  
 133 this simulation also includes a transition toward a dipole field, a significantly lower plasma  
 134 pressure in the lobes of  $\sim 0.5\%$  of the typical lobe magnetic pressure, and a small net  
 135 cross-tail magnetic field component of  $\sim 1\%$  of the lobe magnetic field strength. We will  
 136 focus particularly on two specific energies and on the tail region inside but close to the  
 137 Moon’s distance, as explored by the ARTEMIS satellites.

138 It should be noted that our investigation, due to the properties of the underlying  
 139 MHD simulation, pertains to large-scale plasmoids of several tens of  $R_E$  lengths in the  
 140 Sun-Earth ( $x$ ) direction, as inferred, for instance, by Hones Jr., Birn, et al. (1984) (75-  
 141 150  $R_E$ ) or Scholer, Gloeckler, Hovestadt, et al. (1984) (50-100  $R_E$ ) on the basis of ISEE-  
 142 3 observations out to  $\sim 220 R_E$ . This length represents the typical length of closed loops  
 143 or helical field lines resulting from single x-line reconnection in the near tail combined  
 144 with a distant x-line beyond the Moon’s distance; it provides an upper limit of observed  
 145 scales. Statistical analyses (Moldwin & Hughes, 1992), based on ISEE-3 measurements  
 146 in the near and distant tail, revealed average lengths of  $16.7 \pm 13.0 R_E$  while Geotail  
 147 data in the nearer tail inside of  $\sim 30 R_E$  yielded plasmoid sizes of 3-9  $R_E$  (Håland et al.,  
 148 1999) and  $\sim 4.4 R_E$  (Slavin et al., 2003). Recent MMS observations indicated plasmoids  
 149 or flux ropes of even shorter scales of a few ion inertial lengths (Eastwood et al., 2007;  
 150 Sun et al., 2019), corresponding to  $x$  dimensions of  $\sim 1500$  km or less.

151 There is evidence that large-scale plasmoids move from the near and mid tail to  
 152 the distant tail (e.g., Richardson et al., 1987; Angelopoulos et al., 1995; Slavin et al., 1998,  
 153 1999). However, it is not clear how small-scale islands or flux ropes evolve, whether they  
 154 form prior to merging into big islands or from break-up of larger ones, and whether they  
 155 maintain their identity between the near and the far tail. Both, particle-in-cell (PIC) and  
 156 resistive MHD simulations have shown that long, stretched thin current sheets may de-  
 157 velop small-scale magnetic islands, which subsequently merge into larger ones (e.g., Bhat-  
 158 tacharjee et al., 2009; Daughton et al., 2009). However, these simulations typically start  
 159 from assuming very thin extended current sheets, which may represent an early state prior  
 160 to the major plasmoid ejection or the “postplasmoid plasma sheet” tailward of a large  
 161 departing plasmoid (Richardson et al., 1987). Furthermore, little is known about the as-  
 162 sociation of small-scale plasmoids with energetic particles. While there is some evidence  
 163 that small-scale islands may be effective in accelerating electrons (Chen et al., 2008; Zhong  
 164 et al., 2020), as suggested by Drake et al. (2006), a similar effect on ions has not been  
 165 documented; most likely because their size is too small to trap and quasi-adiabatically  
 166 affect ions.

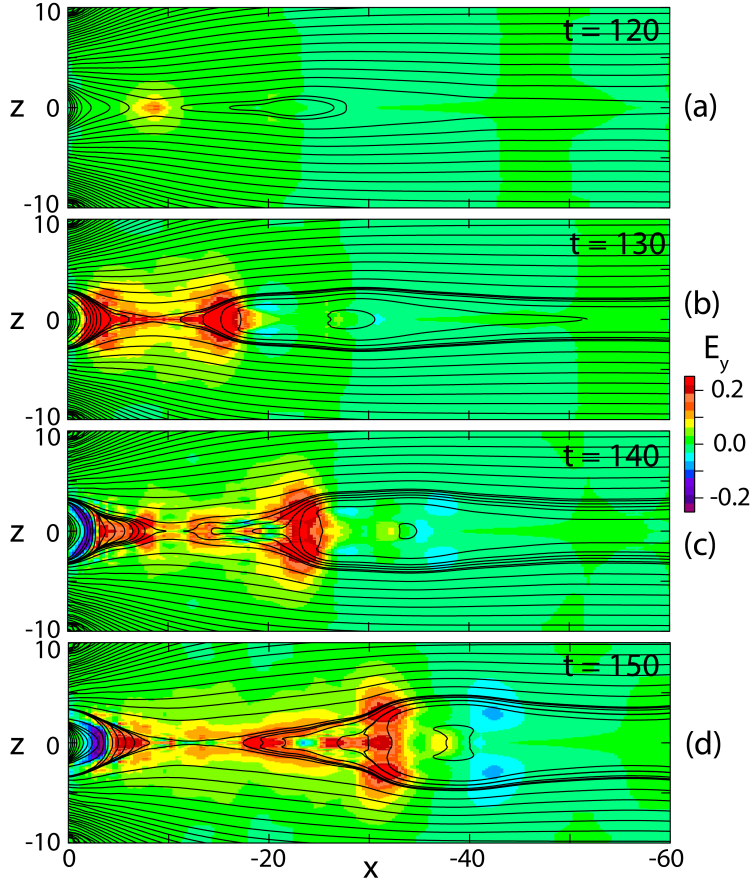


**Figure 1.** Evolution of the (normalized) electric field component  $E_y$  (color) in the  $x, z$  plane. Black lines again are magnetic flux contours.

## 2 MHD Results

The underlying MHD simulation is described in more detail by Birn et al. (2011). It spans a region  $0 \geq x \geq -60$ ,  $|y| \leq 40$ ,  $|z| \leq 10$  with the Earth dipole located at  $x = 5$ , outside the box. As in earlier papers, we use a dimensional length unit  $L_n = 1.5R_E$ , choosing other dimensional units as  $B_n = 12.6$  nT and  $v_n = 1000$  km/s. Here  $B_n$  denotes the lobe field strength and  $v_n$  an Alfvén velocity, based on  $B_n$  and the plasma sheet density, at  $x \approx -10$ , close to the location where the x-line forms in the simulation. The chosen units lead to a time unit  $t_n = L_n/v_n \approx 10$  s and electric field  $E_n = v_n B_n = 12.6$  mV/m.

After a period of external driving, causing the formation of a thin embedded current sheet, a dynamic evolution is initiated at  $t = 61$  by imposing finite resistivity concentrated in the region of enhanced current density, while the driving is stopped. This leads to the start of weak reconnection at  $t \approx 90$ , followed by more rapid reconnection after  $t \approx 120$ .

Figures 1 and 2 provide an overview of the evolution of the cross-tail electric field in the  $y = 0$  and  $z = 0$  plane, respectively. (The Moon’s distance would be close to the center of the box near  $x = -35$ .) This electric field component, closely related to the fast earthward and tailward flows, is the dominant factor in the particle acceleration. The contribution to the total field from the resistive term is confined to the vicinity of

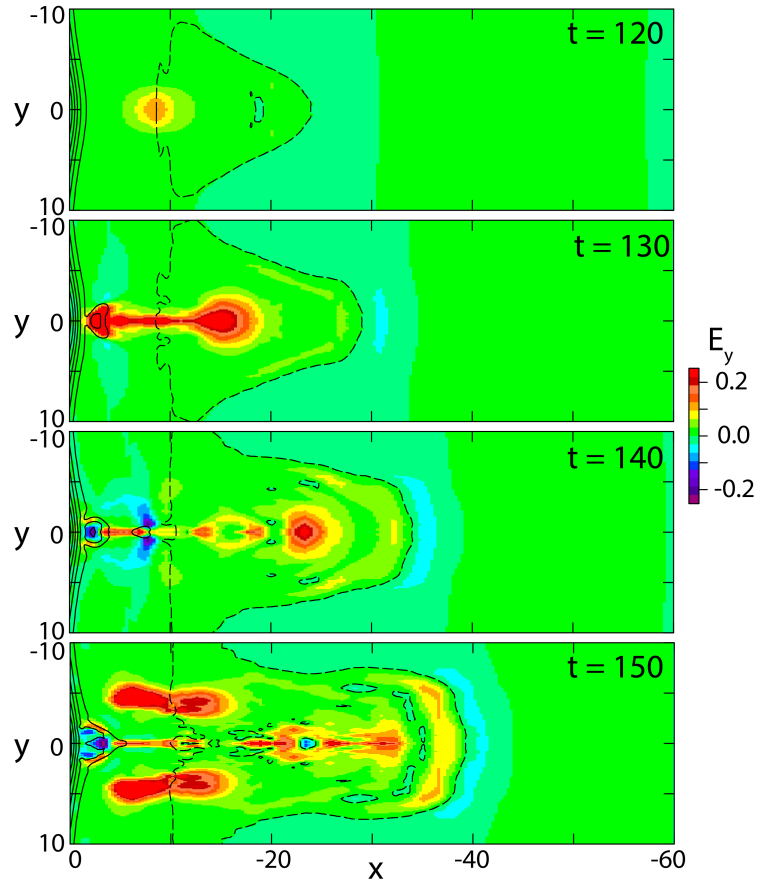


**Figure 2.** Evolution of the (normalized) electric field component  $E_y$  (color) in the  $x, y$  plane. Black lines are contours of constant  $B_z$ ;  $B_z = 0$  lines are dashed. The two blue lines in panel (b) are projections of field lines.

186 the x-line. It is initially considerably smaller than the fields shown and would not show  
 187 in the color scheme of Figures 1 and 2 but is increased at later times over the initial val-  
 188 ues by an intensification of current density associated with the dynamic evolution, which  
 189 might be considered as nonlinear (resistive) tearing in a 3D geometry (Schindler, 1974;  
 190 Galeev, 1979). As the application of an external field is discontinued after the initial driven  
 191 phase, the electric field in the MHD simulation illustrated in Figures 1 and 2 can entirely  
 192 be considered as inductive, resulting from  $\partial\mathbf{B}/\partial t$ .

193 Figure 2 shows the effects of rapid reconnection and fast flows first near midnight  
 194 ( $t = 130, 140$ ) and then ( $t = 150$ ) near  $|y| \approx 4$ . It is noteworthy that the maximum  
 195 cross-tail voltage difference  $\int E_y dy$  tailward of the near-Earth reconnection site ( $x \approx$   
 196  $-10$ ) amounts to  $\sim 80$  kV, based on our chosen units. This corresponds to a maximum  
 197 energy of  $\sim 80$  keV for a singly charged ion gained from a single crossing of the high  $E_y$   
 198 field.

199 Note also that, even before additional flow bursts arise outside of the first one near  
 200 midnight, there is not a uniquely defined plasmoid width in  $y$ , as illustrated by the two  
 201 field line projections in Figure 2b. The field line closer to the core of the plasmoid (dark  
 202 blue line) extends over a wider distance in  $y$  than the field line closer to the plasmoid  
 203 boundary (light blue line).

### 204 3 Orbit Integration

205 Proton orbits were integrated backward in time from selected final locations and  
 206 final velocities on the basis of the time dependent magnetic and electric fields of the MHD  
 207 simulation. The orbits were stopped when they reached the initial state ( $t = 61$ ) or one  
 208 of the outer boundaries. At the inner boundary,  $x = 0$ , particles were reflected back,  
 209 however, taking into account a delay time consistent with mirroring closer to Earth, out-  
 210 side the simulation box. This time was estimated from motion in a Tsyganenko model  
 211 field (Tsyganenko, 1987) that was matched to the inner boundary. Particle fluxes were  
 212 evaluated by mapping the phase space density  $f$  from the initial to the final location,  
 213 using Liouville's theorem of the conservation of  $f$  along a phase space trajectory (Curran  
 214 & Goertz, 1989). Enhanced fluxes therefore are primarily due to large energy gains (low  
 215 initial energies implying higher  $f$  values) and, to a minor extent the higher density in  
 216 the source region, that is, central plasma sheet (CPS) versus plasma sheet boundary layer  
 217 (PSBL) or lobes.

218 Source distributions were chosen as kappa distributions (Vasyliunas, 1968; Christon  
 219 et al., 1988, 1989),

$$220 f(W) \propto n_i \left(1 + \frac{W}{(\kappa - 3/2)kT_i}\right)^{-\kappa-1} \quad (1)$$

221 with  $W$  representing particle energy. The parameters  $n_i$  and  $T_i$  were chosen to be con-  
 222 sistent with the pressure in the MHD simulation and  $\kappa = 5.5$  was chosen on the ba-  
 223 sis of tail observations (Christon et al., 1988, 1989). We note, however, that the results  
 224 reported below mostly reflect the energy gain along the orbits and would not be changed  
 225 qualitatively if different source distributions (say, Maxwellians) or kappa values were cho-  
 226 sen.

226 We used full orbit integration

$$227 \frac{d\mathbf{x}}{dt} = \mathbf{u} \quad \frac{d\mathbf{u}}{dt} = \frac{eB_n t_n}{m} (\mathbf{E} + \mathbf{u} \times \mathbf{B}) \quad (2)$$

228 Here  $\mathbf{x}$  and  $\mathbf{u}$  represent the particle location and velocity, normalized by  $L_n$  and  $v_n$ , re-  
 229 spectively,  $m$  is the ion (here, proton) mass and  $e$  is the proton charge, while  $\mathbf{E}$  and  $\mathbf{B}$   
 230 are the normalized MHD fields, which were interpolated linearly in space and time from  
 231 the finite grid of the MHD simulation. Since this could, in principle, lead to spurious par-  
 232 allel electric fields, we did comparisons with an interpolation procedure that separated

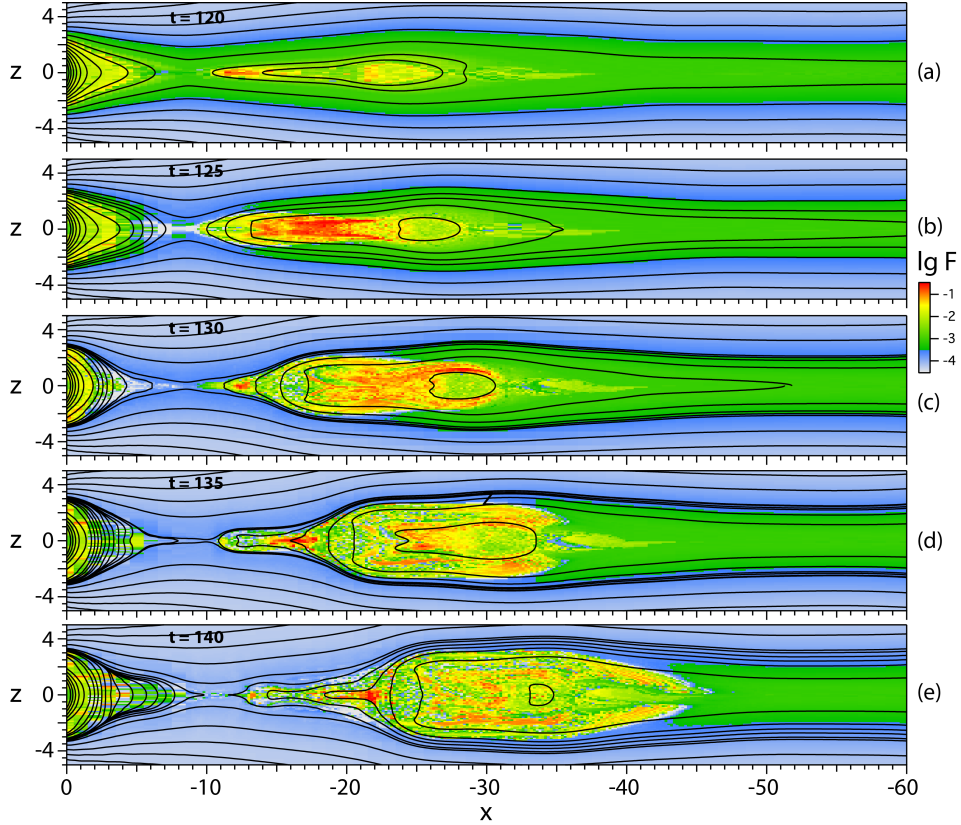


**Figure 3.** Tailward fluxes of 20.9 keV protons in the  $y = 0$  plane.

parallel and perpendicular electric field components and found that this effect was negligible for ion orbits.

Based on the velocity unit defined in section 2, the proton energy is given by  $W = W_n u^2$  where

$$W_n = \frac{1}{2} m v_n^2 = 5.22 \text{ keV} \quad (3)$$

We note that the orbit integration (2) depends only on  $q/m$  (with  $q = e$  for protons), through the dimensionless parameter  $\sigma$  defined by

$$\sigma = \omega_{ci} t_n = \frac{q B_n}{m} t_n = \frac{L_n}{d_i} \quad (4)$$

where  $d_i$  is the ion (proton) inertial length, with  $\sigma = 11.5$  for the chosen units. Multiplying the magnetic field unit by a factor  $\lambda$  and the time unit by  $1/\lambda$ , leaves  $\sigma$  unchanged. Leaving the length unit also unchanged, the orbit results can be applied also to a different parameter set with  $v_n$  multiplied by  $\lambda$ , and  $E_n$  and  $W_n$  by  $\lambda^2$ .

## 4 Evolution of Ion Fluxes

### 4.1 Midnight meridional plane

Figures 3 and 4 show the evolution of tailward fluxes of 20.9 keV and 83.5 keV (final energy), respectively, in the midnight meridional plane,  $y = 0$ . Each pixel corresponds to a single phase space trajectory backward from the given location to the source



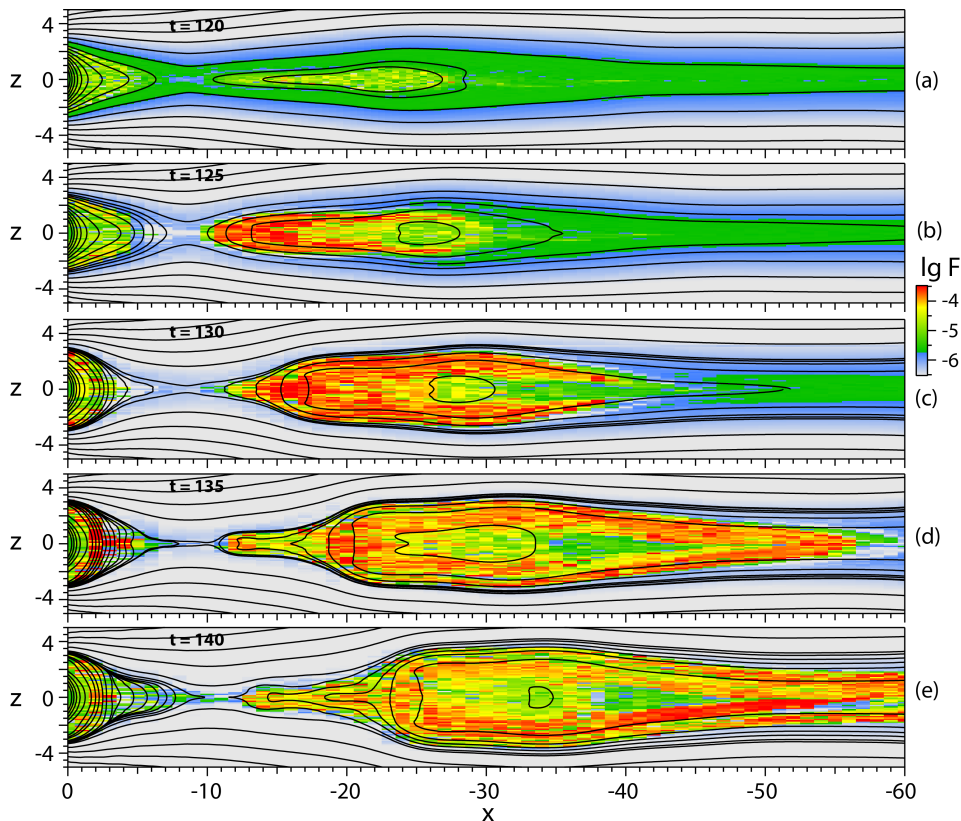


**Figure 4.** Same as Figure 3 but for 83.5 keV energy.

247 location (which in almost all cases was at the initial state  $t = 61$ ) and the distribution  
 248 function value  $f$  thus represents the value at the source location mapped to the final lo-  
 249 cation, according to the procedure described in Section 3. The fluxes occupy the central  
 250 plasma sheet closer to Earth but split into two layers surrounding the plasmoid core  
 251 at later times and larger distances. As expected and observed, the higher-energy fluxes  
 252 are at higher latitude, somewhat closer to the plasmoid boundary. Remarkably, at later  
 253 times and larger distance, the boundary fluxes at higher energy converge around the front  
 254 of the plasmoid toward the equatorial plane. In the present simulation and based on the  
 255 chosen dimensional units, this happens at a distance beyond the Moon's. However, this  
 256 result might vary depending on characteristic length and velocity scales.

## 257 4.2 Equatorial plane

258 Figures 5 and 6 show the evolution of the tailward fluxes in the equatorial plane,  
 259  $z = 0$ , together with the projections of several orbits contributing to the enhanced fluxes,  
 260 shown as multi-colored lines. The color of these lines indicate the instantaneous energy  
 261  $W$  corresponding to the color bars on the lower right in Figure 5 and the top right in  
 262 Figure 6. The green portions, in particular, indicate where the dominant energy increase  
 263 occurs

264 The regions of enhanced fluxes show a complicated structure, which involves mul-  
 265 tiple regions, and changes in time. The enhanced fluxes tend to be shifted toward dusk  
 266 as expected from the duskward acceleration. However, at times enhanced fluxes may also  
 267 extend downward, for instance at  $t = 130$  for 20.9 keV (Figure 5c) near  $x \approx -15$ . In  
 268 this case, the effect appears to be related to an expansion of the region of enhanced elec-

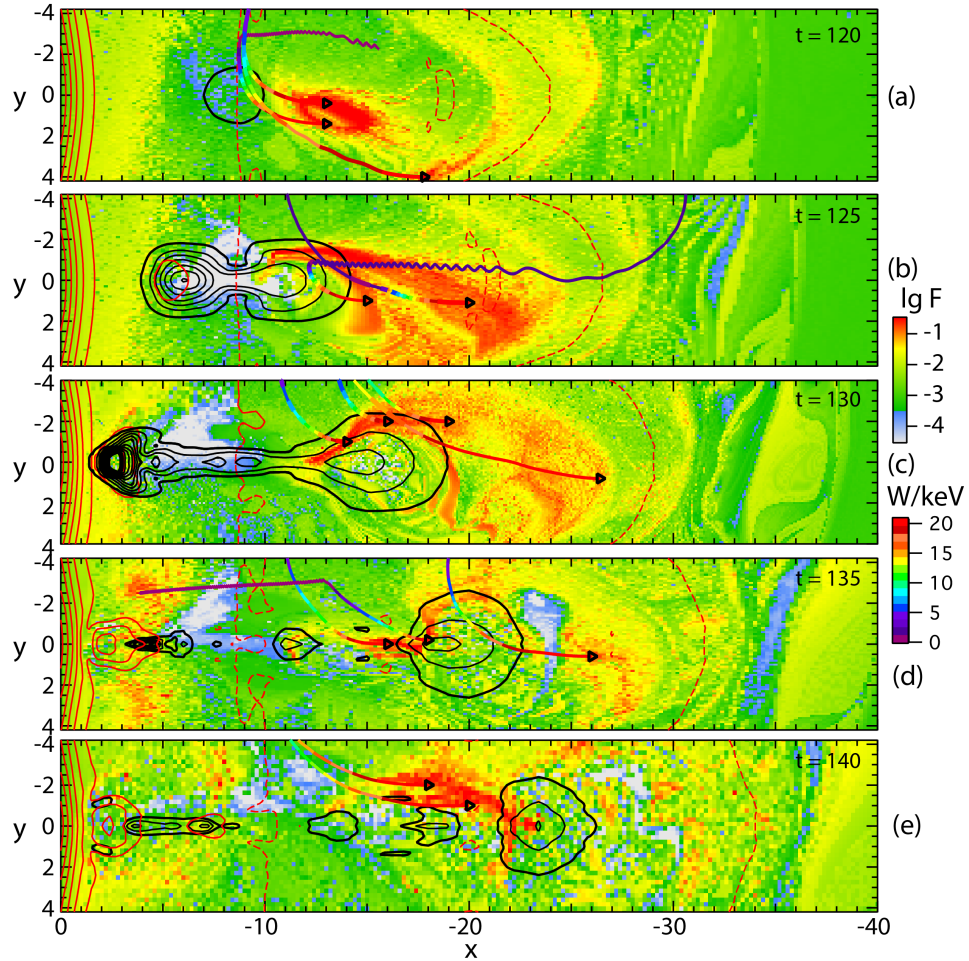


**Figure 5.** Tailward fluxes of 20.9 keV protons in the  $z = 0$  plane at various times indicated in the top right of each panel. Black contours indicate enhanced cross-tail electric field, and red contours are contours of constant  $B_z$ , as shown in Figure 2, with the  $B_z = 0$  lines shown as dashed lines. The multi-colored lines show projections of typical orbits of protons contributing to the enhanced fluxes with the color indicating the instantaneous energy corresponding to the lower scale on the right. The black triangles show the final particle locations.

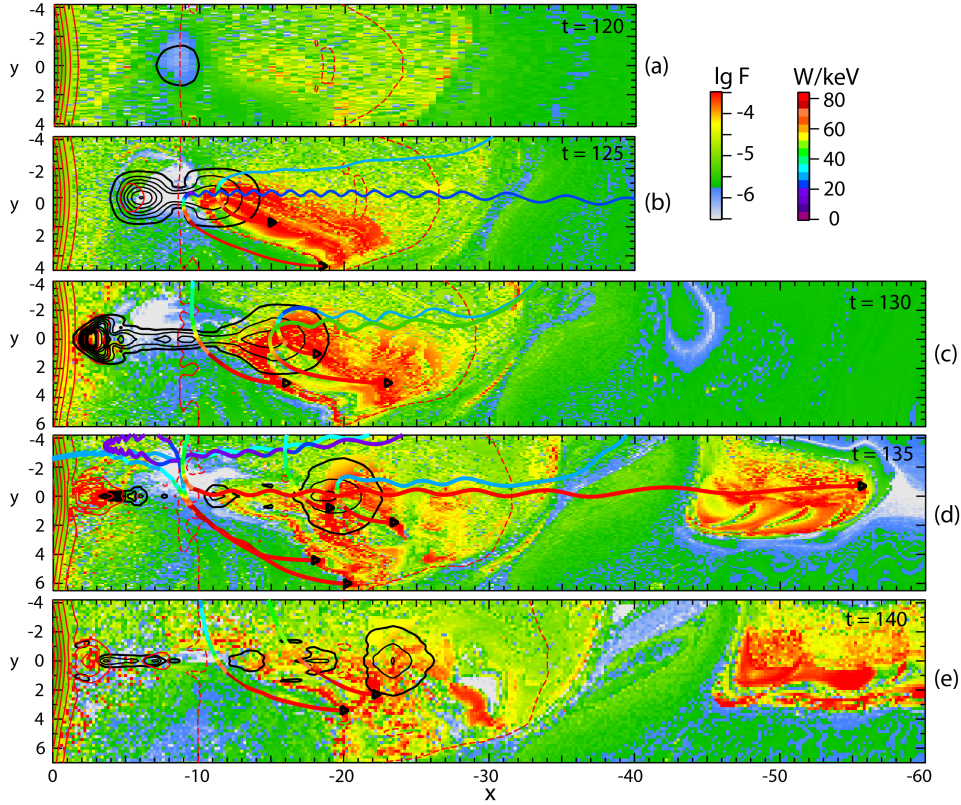


**Figure 6.** Same as Figure 5 but for 83.5 keV energy.

269 tric field  $E_y$  (and the associated flow) from a narrow channel closer to the x-line as indicated by the black contours. The sample orbits in Figure 5c that end on the dawn side indicate that the flux enhancements also result from single crossings of the enhanced electric field in the  $y$  direction. As one might expect, this effect is less pronounced at higher energies (Figure 6). Figures 6d,e also show the sudden appearance of fluxes at large distance,  $x \approx -50$  and beyond, which is related to the convergence of the fluxes toward the equatorial plane shown in Figures 4d,e.

### 276 4.3 Cross-sectional $x = -30$ plane

277 Figure 7 shows the evolution of tailward fluxes of 20.9 keV and 83.5 keV in the center of the box,  $x = -30$ , as function of  $y$  and  $z$ . Black and red contours indicate topological boundaries. The red lines show the outer boundary of closed plasmoid field lines and the black lines the inner lobe boundary. The region between the red and the black lines in the center corresponds to open, disconnected field lines, resulting from lobe field reconnection, whereas the region farther away in  $|y|$  correspond to closed field lines, extending into the more distant tail, which have not (yet) undergone reconnection. Overall the region of energetic particle fluxes show a shape of a lying U, extending duskward and toward the boundary regions near midnight. The outer separatrix (black lines) encloses the region of accelerated particles with the region of more energetic particles closer to the boundaries but the boundary between closed plasmoid fields and open disconnected field lines (red lines) apparently does not affect the energetic particle fluxes. However, this may be the result of our MHD configuration, which has no distinct drop in pressure or density at the open/closed boundary.

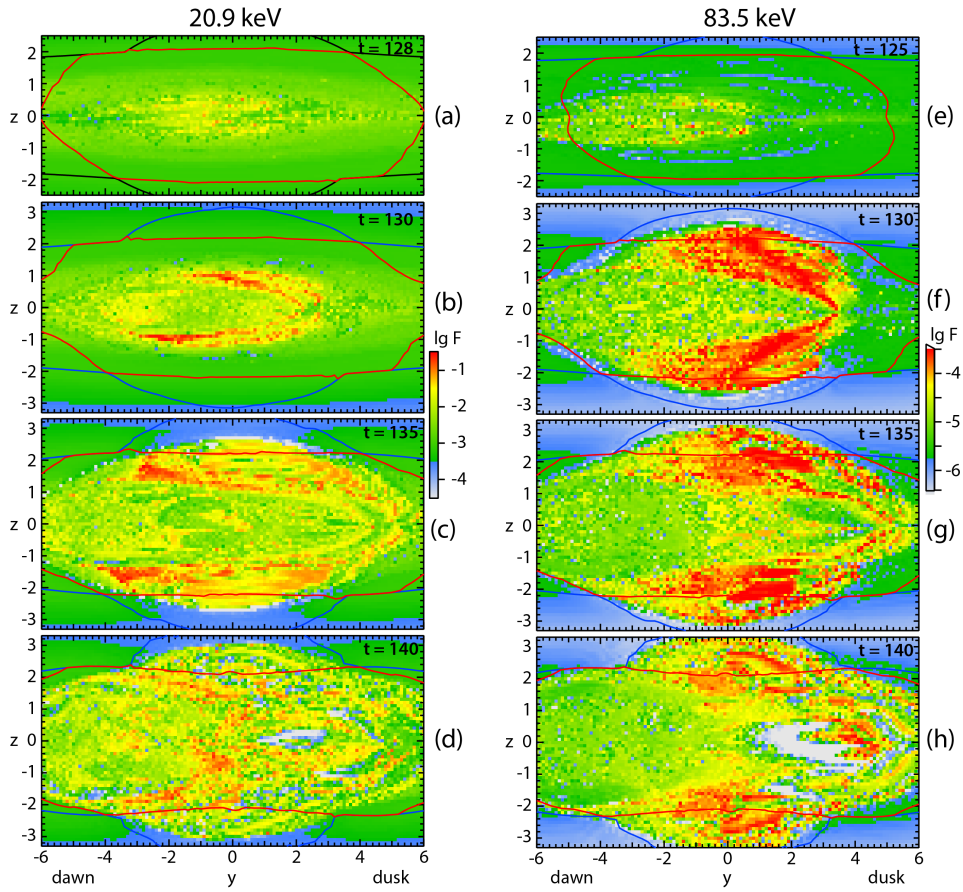


**Figure 7.** Tailward fluxes of 20.9 and 83.5 keV protons in the  $x = -30$  plane. Black and red contours indicate topological boundaries with the red line showing the outer boundary of closed plasmoid field lines and the black line the inner lobe boundary.

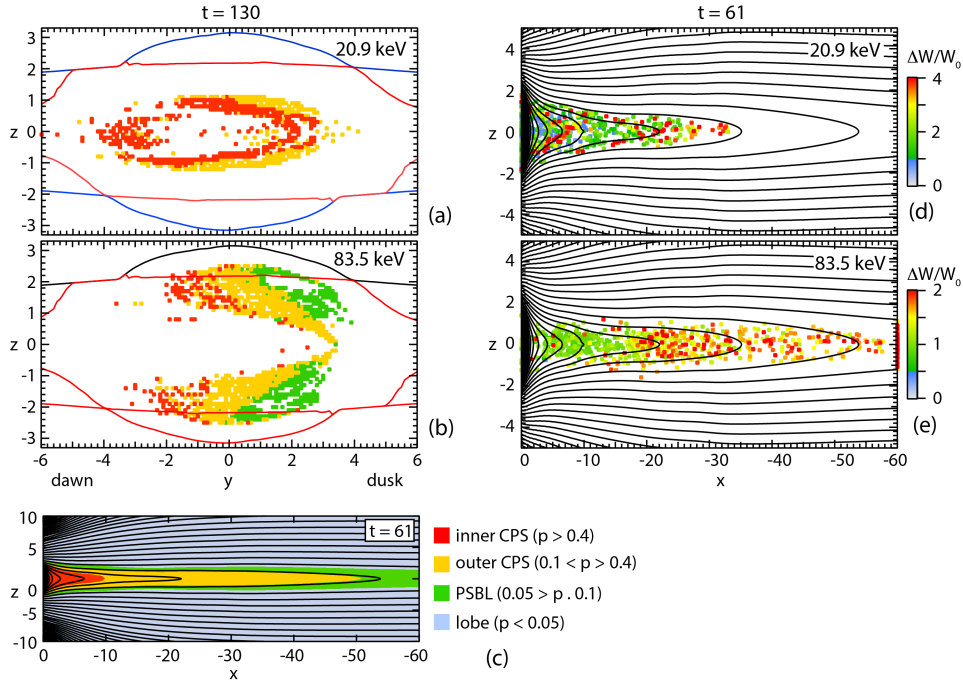


**Figure 8.** Origins of accelerated 20.9 and 83.5 keV protons contributing to enhanced fluxes in the  $x = -30$  plane at  $t = 130$ . Panels a and b show top fluxes in the velocity distributions of Figures 7b,f, with color indicating the origin as defined by the initial pressure (panel c). Panels d and e show the source locations of the particles projected into the  $x, z$  plane with color now indicating the relative energy gain, together with the magnetic flux contours at  $t = 61$ . Black and red contours in panels a and b again indicate the topological boundaries with the red line showing the outer boundary of closed plasmoid field lines and the black line the inner lobe boundary

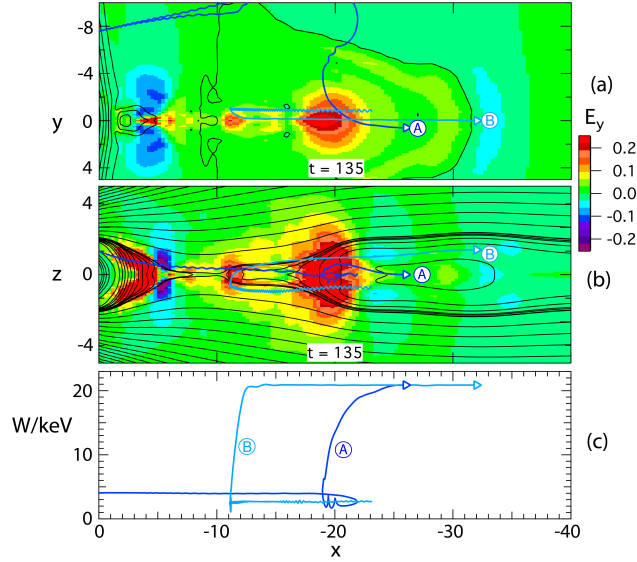


**Figure 9.** Typical orbits of accelerated protons (dark and light blue curves, labeled A and B) contributing to enhanced 20.9 keV fluxes at  $t = 130$  in Figure 7b: (a) projection into the  $x, z$  plane, (b) projection into the  $x, y$  plane. The orbits are superposed on snapshots of the cross-tail electric field  $E_y$  at  $t = 130$ ; the final locations are indicated by small triangles. Panel (c) shows the particle energies above the location in  $x$ .

291 The origins of the accelerated particles shown in Figure 7c and g at  $t = 130$  are  
 292 indicated in Figure 8a,b, selecting the pixels with the largest fluxes. The origins are col-  
 293 ored according to the initial pressure at  $t = 61$ , as indicated by panel c. The 20.9 keV  
 294 particles (Figure 8a) all originate from the inner (red) and outer (orange pixels) CPS,  
 295 while for 83.5 keV (Figure 8b) the PSBL contributes as well (green pixels). These con-  
 296 tributions are well ordered, proceeding duskward and outward with the sources proceed-  
 297 ing from inner CPS toward outer CPS and PSBL. It is noteworthy that the boundaries  
 298 between these source regions are not related to the boundary between closed plasmoid  
 299 and disconnected field lines (red lines) at this time.

300 Figures 8d and e show the source locations in  $x$  and  $z$  of the particles contribut-  
 301 ing to the peak fluxes. The color now indicates the relative energy gain of the particles.  
 302 This shows that particles with the higher energy gain tend to come from the more dis-  
 303 tant tail for 83.5 keV (orange and red pixels in Figure 8e) while the source locations are  
 304 more mixed for 20.9 keV (Figure 8d).

## 305 5 Typical Orbits and Acceleration Mechanisms

306 The orbits shown in Figure 5 and 6 already illustrate that the energy gain typically  
 307 results from a single crossing of the enhanced electric field region; the acceleration re-  
 308 gion primarily correspond to the part of the orbits colored in green. The acceleration may  
 309 be close to the x-line, near  $x = -10$ , or farther tailward within the departing plasmoid.  
 310 Here we illustrate two orbits in more detail.

311 Figure 9 shows two characteristic orbits (dark and light blue lines with final loca-  
 312 tions indicated by small triangles) contributing to the enhanced 20.9 keV fluxes at  $t =$   
 313 135, as shown in Figures 3d and 5d, superposed on the color-coded electric field  $E_y$  at  
 314 the final time. Figure 9a shows projections of the orbits into the  $x, y$  plane, Figure 9b

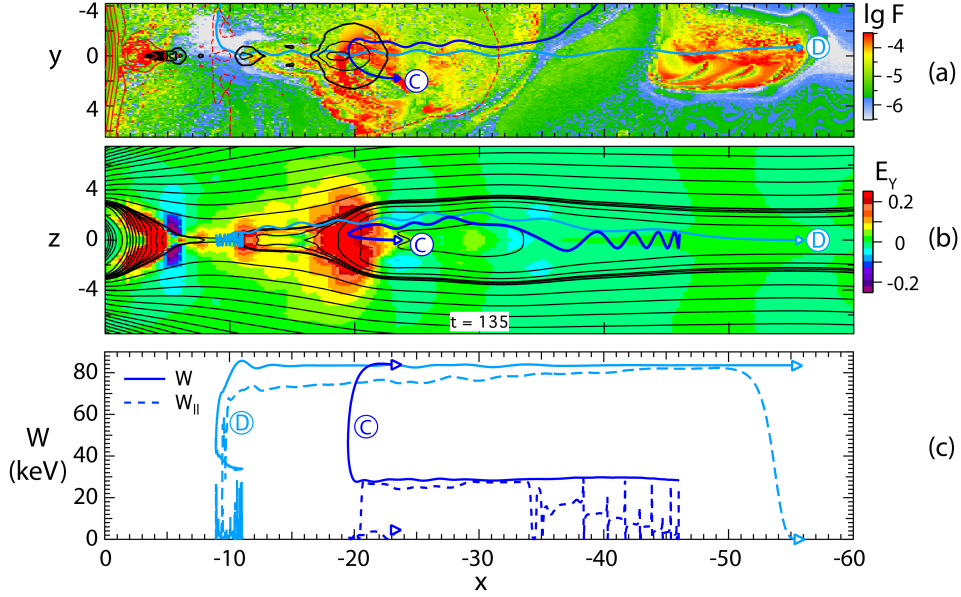


**Figure 10.** Same as Figure 9 but for protons contributing to enhanced fluxes at 83.5 keV. Panel a shows the color-coded particle fluxes in the  $x, y$  plane as in Figure 6d while panel b shows the electric field  $E_y$ . Panel c shows the particle energies as function of  $x$  as solid lines and the field-aligned contributions as dashed lines.

in the  $x, z$  plane. The bottom panel, Figure 9c shows the energy as function of location  $x$ . It clearly demonstrates that the acceleration occurs by single crossings of the acceleration region of enhanced cross-tail electric field, close to the x-line for orbit A (light blue) but farther tailward in the moving plasmoid for orbit B (dark blue line). In either case the initial energy is near or below the thermal energy  $W_n = 5.2$  keV. As shown by panel b, orbit A represents a particle contributing to the beams on the outside of the plasmoid near the boundary, while the particle of orbit B contributes to the equatorial fluxes.

Figure 10 illustrates two representative orbits of accelerated ions of 83.5 keV final energy. Both ions originate from the central plasma sheet on meandering orbits but from different distances. Particle A (dark blue line) is characteristic for those contributing to the enhanced flux around  $x \approx -50$ , resulting from the convergence of boundary layer fluxes toward the equatorial plane. As illustrated by panel b, this particle in fact contributes to the boundary fluxes at earlier times. Panel c demonstrates that the particle energy is almost entirely field-aligned after cross-tail acceleration near the x-line at  $x \approx -10$  before it converges toward  $z = 0$  and becomes perpendicular when it reaches the equatorial plane (dark blue dashed line).

In contrast, particle B originates from a more distant location in  $x$  and becomes accelerated when it encounters the enhanced electric field of the departed plasmoid near  $\approx -20$ . In both cases the initial energy is  $\sim 30$  keV, consistent with the fact that the maximum gain by a simple crossing of the acceleration region should be less than about 80 keV.

All sample orbits shown so far demonstrate the same acceleration mechanism, a simple, non-adiabatic, crossing of a region of enhanced cross-tail electric field, either near the x-line in the near tail or within the departing plasmoid. This provides a maximum

340 for the possible acceleration of  $\sim 80$  keV, based on the chosen parameters, but more typ-  
 341 ically 50 keV or less.

## 342 6 Summary and Discussion

343 We have used our combined MHD/test particle approach to explore the acceler-  
 344 ation and flux increases of hydrogen ions in the mid tail region tailward of a near-Earth  
 345 reconnection site. External driving is used in the MHD simulation only to prepare the  
 346 tail for reconnection by the formation of a thin embedded current sheet in the near tail.  
 347 This driving is discontinued after finite resistivity is imposed in the region of the thin  
 348 current sheet to enable reconnection; hence the simulation does not include a general ex-  
 349 ternally driven convection. Our simulation includes a small net cross-tail magnetic field  
 350 (guide field) of a few percent of the lobe field, which breaks the mirror symmetry but  
 351 apparently has no significant influence on the dynamic evolution. The simulation does  
 352 not include a distant reconnection site. Therefore the investigated properties are purely  
 353 the consequences of near-Earth reconnection and tailward plasmoid ejection; they do not  
 354 include fast impulsive or convective earthward flows in the mid tail, which in observa-  
 355 tions may constitute about one half of the fast flows at lunar distance (Kiehas et al., 2018).

356 Concerning the MHD simulation, we would like to point out a few results. First,  
 357 although the maximum tailward speeds are comparable to the earthward speeds in the  
 358 inner tail, the maximum integrated cross-tail electric fields in the departing plasmoid are  
 359 smaller than in the dipolarizing flux bundle moving earthward, yielding cross-tail volt-  
 360 ages of approximately 50-80 keV compared to  $\sim 200$  keV on the earthward side for the  
 361 chosen parameters (Section 2). Secondly, the simulation does not yield a unique plas-  
 362 moid width. The helical field lines close to the core of the plasmoid tend to extend more  
 363 widely in  $y$ , and are more tightly wound, than the field lines on the outside, even when  
 364 both kinds are still connected to the Earth at both ends. The narrower width of the outer  
 365 structure is related to the width of the fast tailward beam and the associated limited width  
 366 of fast reconnection.

367 We have focused on two final energies, 20.9 and 83.5 keV, the latter being slightly  
 368 above the maximum energy gain from a crossing of the dawn-dusk electric field region  
 369 associated with the reconnection site and the departing plasmoid, which is about 50-80  
 370 keV, based on the chosen dimensional units. We note again, that our results can still be  
 371 scaled to different cases by choosing different normalization parameters. For instance,  
 372 increasing the magnetic field unit by, say, a factor of 2 and reducing the time unit by 1/2  
 373 leaves the dimensionless orbit results unchanged but would increase the two chosen par-  
 374 ticle energies to 83.5 and 334 keV, respectively, and the cross tail voltage to  $\sim 200$ -320  
 375 kV.

376 The following are major conclusions

- 377 1. The ion acceleration is primarily due to direct acceleration across the tail from the  
 378 inductive electric field associated with the dynamic tail evolution, involving near-  
 379 tail reconnection and plasmoid ejection. This electric field is dominated by the res-  
 380 istive term only in the immediate vicinity of the x-line but elsewhere given by the  
 381 motional  $-\mathbf{v} \times \mathbf{B}$  field. The maximum acceleration is thus limited by the maxi-  
 382 mum cross-tail voltage  $\int E_y dy$ . This is about 80 kV for the chosen parameters but  
 383 might be higher in different scenarios when different parameters (larger  $B_n$  and/or  
 384 larger  $L_n$ ) were more appropriate. This is lower than what we found for the earth-  
 385 ward side. The primary reason is that in our simulation, the  $B_z$  field associated  
 386 with the plasmoid is smaller than the field in the earthward propagating dipolar-  
 387 ization front. Our simulation does not exhibit the enhanced fields of anti-dipolarization  
 388 fronts, which are occasionally observed on the tailward side (Li et al., 2014) and  
 389 could possibly lead to larger cross-tail voltages.



- 390 2. The spatial distributions in the  $x, z$  plane show the boundary layers of tailward  
 391 streaming energetic ions, as expected from ISEE-3 observations (Scholer et al., 1983;  
 392 Scholer, 1984; Hones Jr., Birn, et al., 1984; Richardson & Cowley, 1985).
- 393 3. The distributions in the  $x, y$  plane are more complicated, but preferentially duskward,  
 394 as to be expected from the acceleration in that direction.
- 395 4. Acceleration of ions may occur anywhere across the tailward propagating electric  
 396 field pulse associated with the plasmoid departure. Different branches of accel-  
 397 erated ions in the equatorial plane can be attributed to different acceleration lo-  
 398 cations in  $x$ . However, field-aligned beams near the plasma sheet boundary are  
 399 primarily accelerated near the x-line in the near tail.
- 400 5. The accelerated particles originate mostly from the central plasma sheet; this is  
 401 a main difference from the results of Scholer and Jamitzky (1989). It is probably  
 402 related to the fact that the Scholer and Jamitzky (1989) simulation was two-dimensional  
 403 without cross-tail variation, while ours is three-dimensional yielding a finite cross-  
 404 tail extent of the reconnection site, the ejected plasmoid, and the associated elec-  
 405 tric fields. In this paper we did not explore entry and acceleration mechanisms for  
 406 different ion species. However, the two possible entry ways might explain the ap-  
 407 parent mixing of ions of ionospheric and solar wind origin observed by Lui et al.  
 408 (1998).

### 409 Acknowledgments

410 The simulation work was performed at Los Alamos under the auspices of the US Depart-  
 411 ment of Energy, supported by NASA grants 80NSSC18K0834, 80NSSC18K1452, and NSF  
 412 grant 1602655. Simulation results are available under doi:10.5281/zenodo.5206828. IJC  
 413 and DLT were supported by the Magnetospheric Multiscale (MMS) mission of NASA's  
 414 Science Directorate Heliophysics Division via subcontract to the Southwest Research In-  
 415 stitute (NNG04EB99C). AR was supported by NASA LWS grant 80NSSC20K1788 and  
 416 the HERMES DRIVE Science center (grant 80NSSC20K0604). JAS was supported by  
 417 NASA's MMS Guest Investigator Program grant 80NSSC18K1363.

### 418 References

- 419 Angelopoulos, V. (2008). The THEMIS mission. *Space Science Reviews*, *141*, 5–34.  
 420 doi: 10.1007/s11214-008-9336-1
- 421 Angelopoulos, V. (2011). The ARTEMIS mission. *Space Science Reviews*, *165*, 3–25.  
 422 doi: 10.1007/s11214-010-9687-2
- 423 Angelopoulos, V., Mitchell, D. G., Williams, D. J., McEntire, R. W., Lui, A. T. Y.,  
 424 Decker, R. B., ... Hayashi, K. (1995). Growth and evolution of a plasmoid  
 425 associated with a small, isolated substorm: IMP 8 and GEOTAIL measure-  
 426 ments in the magnetotail. *Geophysical Research Letters*, *22*(22), 3011-3014.  
 427 doi: <https://doi.org/10.1029/95GL03133>
- 428 Armstrong, T. P., & Krimigis, S. M. (1968). Observations of protons in the magne-  
 429 tosphere and magnetotail with Explorer 33. *Journal of Geophysical Research*,  
 430 *73*(1), 143-152. doi: <https://doi.org/10.1029/JA073i001p00143>
- 431 Atkinson, G. (1966). A theory of polar substorms. *J. Geophys. Res.*, *71*, 5157-5164.
- 432 Atkinson, G. (1967). Polar magnetic substorms. *J. Geophys. Res.*, *72*, 1491-1494.
- 433 Baker, D. N., Bame, S. J., Birn, J., Feldman, W. C., Gosling, J. T., Hones Jr.,  
 434 E. W., ... Sibeck, D. G. (1984). Direct observations of passages of the  
 435 distant neutral line (80-140  $R_E$ ) following substorm onsets: ISEE-3. *Geo-*  
 436 *physical Research Letters*, *11*(10), 1042-1045. doi: [https://doi.org/10.1029/  
 437 GL011i010p01042](https://doi.org/10.1029/GL011i010p01042)
- 438 Baker, D. N., Pulkkinen, T. I., Angelopoulos, V., Baumjohann, W., & McPherron,  
 439 R. L. (1996). Neutral line model of substorms: Past results and present view.  
 440 *J. Geophys. Res.*, *101*, 12975-13010.

- 441 Bame, S. J., Anderson, R. C., Asbridge, J. R., Baker, D. N., Feldman, W. C.,  
 442 Gosling, J. T., ... Zwickl, R. D. (1983). Plasma regimes in the deep geo-  
 443 magnetic tail: ISEE 3. *Geophysical Research Letters*, *10*(9), 912-915. doi:  
 444 <https://doi.org/10.1029/GL010i009p00912>
- 445 Behannon, K. W. (1968). Mapping of the Earth's bow shock and magnetic tail by  
 446 Explorer 33. *Journal of Geophysical Research*, *73*(3), 907-930. doi: [https://doi](https://doi.org/10.1029/JA073i003p00907)  
 447 [.org/10.1029/JA073i003p00907](https://doi.org/10.1029/JA073i003p00907)
- 448 Bhattacharjee, A., Huang, Y.-M., Yang, H., & Rogers, B. (2009). Fast reconnection  
 449 in high-Lundquist-number plasmas due to the plasmoid instability. *Physics*  
 450 *of Plasmas*, *16*(11), 112102. Retrieved from [https://doi.org/10.1063/](https://doi.org/10.1063/1.3264103)  
 451 [1.3264103](https://doi.org/10.1063/1.3264103) doi: 10.1063/1.3264103
- 452 Birn, J., & Hesse, M. (1996). Details of current disruption and diversion in simula-  
 453 tions of magnetotail dynamics. *J. Geophys. Res.*, *101*, 15345.
- 454 Birn, J., Nakamura, R., Panov, E., & Hesse, M. (2011). Bursty bulk flows and dipol-  
 455 arization in MHD simulations of magnetotail reconnection. *J. Geophys. Res.*,  
 456 *116*. doi: 10.1029/2010JA016083
- 457 Birn, J., Thomsen, M. F., & Hesse, M. (2004). Acceleration of oxygen ions in the  
 458 dynamic magnetotail. *Annales Geophysicae*, *22*(4), 1305-1315. doi: 10.5194/  
 459 [angeo-22-1305-2004](https://doi.org/10.5194/angeo-22-1305-2004)
- 460 Burch, J. L., Moore, T. E., Torbert, R. B., & Giles, B. L. (2016). Magnetospheric  
 461 Multiscale: Overview and science objectives. *Space Sci. Rev.*, *199*, 5-21. doi:  
 462 [10.1007/s11214-015-0164-9](https://doi.org/10.1007/s11214-015-0164-9)
- 463 Chen, L.-J., Bhattacharjee, A., Puhl-Quinn, P. A., Yang, H., Bessho, N., Imada, S.,  
 464 ... Georgescu, E. (2008). Observation of energetic electrons within magnetic  
 465 islands. *Nature Physics*, *4*(1), 19-23.
- 466 Christon, S. P., Mitchell, D. G., Williams, D. J., Huang, C. Y., Frank, L. A., &  
 467 Eastman, T. E. (1988). Energy spectra of plasma sheet ions and electrons from  
 468 ~ 50eV/e to 1 MeV during plasma sheet temperature transitions. *J. Geophys.*  
 469 *Res.*, *93*, 2562.
- 470 Christon, S. P., Williams, D. J., Mitchell, D. G., Frank, L. A., & Huang, C. Y.  
 471 (1989). Spectral characteristics of plasma sheet ion and electron populations  
 472 during undisturbed geomagnetic conditions. *J. Geophys. Res.*, *94*, 13,409.
- 473 Cowley, S. W. H., Hynds, R. J., Richardson, I. G., Daly, P. W., Sanderson, T. R.,  
 474 Wenzel, K.-P., ... Tsurutani, B. T. (1984). Energetic ion regimes in the deep  
 475 geomagnetic tail: ISEE-3. *Geophysical Research Letters*, *11*(3), 275-278. doi:  
 476 <https://doi.org/10.1029/GL011i003p00275>
- 477 Curran, D. B., & Goertz, C. K. (1989). Particle distributions in a two-dimensional  
 478 reconnection field geometry. *J. Geophys. Res.*, *94*, 272.
- 479 Daly, P. W., Sanderson, T. R., & Wenzel, K.-P. (1984). Survey of energetic ( $E >$   
 480 35 keV) ion anisotropies in the deep geomagnetic tail. *Journal of Geophysical*  
 481 *Research: Space Physics*, *89*(A12), 10733-10739. doi: [https://doi.org/10.1029/](https://doi.org/10.1029/JA089iA12p10733)  
 482 [JA089iA12p10733](https://doi.org/10.1029/JA089iA12p10733)
- 483 Daughton, W., Roytershteyn, V., Albright, B. J., Karimabadi, H., Yin, L., & Bow-  
 484 ers, K. J. (2009). Transition from collisional to kinetic regimes in large-  
 485 scale reconnection layers. *Phys. Rev. Lett.*, *103*, 065004. Retrieved from  
 486 <https://link.aps.org/doi/10.1103/PhysRevLett.103.065004> doi:  
 487 [10.1103/PhysRevLett.103.065004](https://doi.org/10.1103/PhysRevLett.103.065004)
- 488 Drake, J. F., Swisdak, M., Che1, H., & Shay, M. A. (2006). Electron acceleration  
 489 from contracting magnetic islands during reconnection. *Nature*, *443*, 553-556.  
 490 doi: 10.1038/nature05116
- 491 Eastwood, J. P., Phan, T.-D., Mozer, F. S., Shay, M. A., Fujimoto, M., Retinò,  
 492 A., ... Dandouras, I. (2007). Multi-point observations of the Hall electro-  
 493 magnetic field and secondary island formation during magnetic recon-  
 494 nection. *Journal of Geophysical Research: Space Physics*, *112*(A6). doi:  
 495 <https://doi.org/10.1029/2006JA012158>

- 496 Escoubet, C. P., Fehringer, M., & Goldstein, M. L. (2001). The Cluster mission.  
497 *Ann. Geophys.*, *19*, 1197.
- 498 Fennell, J. F. (1970). Observations of proton bursts in the magnetotail with Ex-  
499 plorer 35. *Journal of Geophysical Research*, *75*(34), 7048-7059. doi: [https://doi](https://doi.org/10.1029/JA075i034p07048)  
500 [.org/10.1029/JA075i034p07048](https://doi.org/10.1029/JA075i034p07048)
- 501 Galeev, A. A. (1979). Reconnection in the magnetotail. *Space Science Rev.*, *23*, 411-  
502 425.
- 503 Grigorenko, E. E., Runov, A., Angelopoulos, V., & Zelenyi, L. M. (2019). Par-  
504 ticle beams in the vicinity of magnetic separatrix according to near-lunar  
505 ARTEMIS observations. *Journal of Geophysical Research: Space Physics*,  
506 *124*(3), 1883-1903. doi: <https://doi.org/10.1029/2018JA026160>
- 507 Håland, S., Sraas, F., & Ullaland, S. (1999). Propagation velocities and dimensions  
508 of plasmoid structures in the near-earth magnetotail. *Geophysical Research*  
509 *Letters*, *26*(21), 3269-3272. doi: <https://doi.org/10.1029/1999GL003609>
- 510 Hones Jr., E. W. (1977). Substorm processes in the magnetotail: Comments on "On  
511 hot tenuous plasmas, fireballs, and boundary layers in the Earth's magneto-  
512 tail" by frank et al. *J. Geophys. Res.*, *82*, 5633.
- 513 Hones Jr., E. W., Baker, D. N., Bame, S. J., Feldman, W. C., Gosling, J. T., McCo-  
514 mas, D. J., ... Tsurutani, B. T. (1984). Structure of the magnetotail at 220  
515  $R_E$  and its response to geomagnetic activity. *Geophysical Research Letters*,  
516 *11*(1), 5-7. doi: <https://doi.org/10.1029/GL011i001p00005>
- 517 Hones Jr., E. W., Birn, J., Baker, D. N., Bame, S. J., Feldman, W. C., McComas,  
518 D. J., ... Tsurutani, B. T. (1984). Detailed examination of a plasmoid in  
519 the distant magnetotail with isee 3. *Geophysical Research Letters*, *11*(10),  
520 1046-1049. doi: <https://doi.org/10.1029/GL011i010p01046>
- 521 Ieda, A., Machida, S., Mukai, T., Saito, Y., Yamamoto, T., Nishida, A., ...  
522 Kokubun, S. (1998). Statistical analysis of the plasmoid evolution with Geo-  
523 tail observations. *Journal of Geophysical Research: Space Physics*, *103*(A3),  
524 4453-4465. doi: <https://doi.org/10.1029/97JA03240>
- 525 Kiehas, S. A., Runov, A., Angelopoulos, V., Hietala, H., & Korovinskiy, D. (2018).  
526 Magnetotail fast flow occurrence rate and dawn-dusk asymmetry at  $x_{GSM} \sim$   
527  $-60r_e$ . *J. Geophys. Res.*, *123*, 17671778. doi: [10.1002/2017JA024776](https://doi.org/10.1002/2017JA024776)
- 528 Kokubun, S., Yamamoto, T., Acuña, M. H., Hayashi, K., Shiokawa, K., & Kawano,  
529 H. (1994). The GEOTAIL magnetic field experiment. *Journal of Geomag-*  
530 *netism and Geoelectricity*, *46*(1), 7-21.
- 531 Li, S.-S., Liu, J., Angelopoulos, V., Runov, A., Zhou, X.-Z., & Kiehas, S. A. (2014).  
532 Antidipolarization fronts observed by ARTEMIS. *Journal of Geophysi-*  
533 *cal Research: Space Physics*, *119*, 71817198. doi: [https://doi.org/10.1002/](https://doi.org/10.1002/2014JA020062)  
534 [2014JA020062](https://doi.org/10.1002/2014JA020062)
- 535 Lui, A. T. Y., Williams, D. J., McEntire, R. W., Christon, S. P., Eastman, T. E.,  
536 Yamamoto, T., & Kokubun, S. (1998). Ion composition and charge state of  
537 energetic particles in flux ropes/plasmoids. *Journal of Geophysical Research:*  
538 *Space Physics*, *103*(A3), 4467-4475. doi: <https://doi.org/10.1029/97JA02256>
- 539 Machida, S., Ieda, A., Mukai, T., Saito, Y., & Nishida, A. (2000). Statisti-  
540 cal visualization of Earth's magnetotail during substorms by means of  
541 multidimensional superposed epoch analysis with Geotail data. *Jour-*  
542 *nal of Geophysical Research: Space Physics*, *105*(A11), 25291-25303. doi:  
543 <https://doi.org/10.1029/2000JA900064>
- 544 Machida, S., Mukai, T., Saito, Y., Obara, T., Yamamoto, T., Nishida, A., ...  
545 Kokubun, S. (1994). GEOTAIL low energy particle and magnetic field ob-  
546 servations of a plasmoid at  $x_{GSM} = -142R_E$ . *Geophysical Research Letters*,  
547 *21*(25), 2995-2998. doi: <https://doi.org/10.1029/94GL02241>
- 548 McPherron, R. L., Russell, C. T., & Aubry, M. A. (1973). Satellite studies of mag-  
549 netospheric substorms on August 15, 1968, 9, Phenomenological model for  
550 substorms. *J. Geophys. Res.*, *78*, 3131-3149.

- 551 Mihalov, J. D., Colburn, D. S., Currie, R. G., & Sonett, C. P. (1968). Configuration  
552 and reconnection of the geomagnetic tail. *Journal of Geophysical Research*,  
553 *73*(3), 943-959. doi: 10.1029/JA073i003p00943
- 554 Mihalov, J. D., & Sonett, C. P. (1968). The cislunar geomagnetic tail gradient in  
555 1967. *Journal of Geophysical Research; Space physics*, *73*(21), 6837-6840. doi:  
556 10.1029/JA073i021p06837
- 557 Moldwin, M. B., & Hughes, W. J. (1992). On the formation and evolution of  
558 plasmoids: A survey of ISEE 3 geotail data. *Journal of Geophysical Re-*  
559 *search: Space Physics*, *97*(A12), 19259-19282. doi: [https://doi.org/10.1029/](https://doi.org/10.1029/92JA01598)  
560 [92JA01598](https://doi.org/10.1029/92JA01598)
- 561 Mukai, T., Machida, S., Saito, Y., Hirahara, M., Terasawa, T., Kaya, N., ...  
562 Nishida, A. (1994). The low-energy particle (LEP) experiment onboard  
563 the GEOTAIL satellite. *Journal of Geomagnetism and Geoelectricity*, *46*(10),  
564 909-909.
- 565 Nagai, T., Takahashi, K., Kawano, H., Yamamoto, T., Kokubun, S., & Nishida,  
566 A. (1994). Initial GEOTAIL survey of magnetic substorm signatures in  
567 the magnetotail. *Geophysical Research Letters*, *21*(25), 2991-2994. doi:  
568 <https://doi.org/10.1029/94GL01420>
- 569 Ness, N. F., Behannon, K. W., Scarce, C. S., & Cantarano, S. C. (1967a). Early  
570 results from the magnetic field experiment on lunar explorer 35. *Journal*  
571 *of Geophysical Research*, *72*(23), 5769-5778. doi: [https://doi.org/10.1029/](https://doi.org/10.1029/JZ072i023p05769)  
572 [JZ072i023p05769](https://doi.org/10.1029/JZ072i023p05769)
- 573 Ness, N. F., Behannon, K. W., Scarce, C. S., & Cantarano, S. C. (1967b).  
574 Eobservations of Earth's magnetic tail and neutral sheet at 510,000 kilo-  
575 meters by explorer 33. *Journal of Geophysical Research*, *72*, 927. doi:  
576 10.1029/JZ072i003p00927
- 577 Nishida, A. (1994). The Geotail mission. *Geophysical Research Letters*, *21*(25),  
578 2871-2873. doi: <https://doi.org/10.1029/94GL01223>
- 579 Richardson, I. G., & Cowley, S. W. H. (1985). Plasmoid-associated energetic ion  
580 bursts in the deep geomagnetic tail: Properties of the boundary layer. *Journal*  
581 *of Geophysical Research: Space Physics*, *90*(A12), 12133-12158. doi: [https://](https://doi.org/10.1029/JA090iA12p12133)  
582 [doi.org/10.1029/JA090iA12p12133](https://doi.org/10.1029/JA090iA12p12133)
- 583 Richardson, I. G., Cowley, S. W. H., Hones Jr., E. W., & Bame, S. J. (1987).  
584 Plasmoid-associated energetic ion bursts in the deep geomagnetic tail: Proper-  
585 ties of plasmoids and the postplasmoid plasma sheet. *Journal of Geophysical*  
586 *Research: Space Physics*, *92*(A9), 9997-10013. doi: [https://doi.org/10.1029/](https://doi.org/10.1029/JA092iA09p09997)  
587 [JA092iA09p09997](https://doi.org/10.1029/JA092iA09p09997)
- 588 Runov, A., Angelopoulos, V., Artemyev, A., Lu, S., & Zhou, X.-Z. (2018). Near-  
589 Earth reconnection ejecta at lunar distances. *Journal of Geophysical Re-*  
590 *search: Space Physics*, *123*(4), 2736-2744. doi: [https://doi.org/10.1002/](https://doi.org/10.1002/2017JA025079)  
591 [2017JA025079](https://doi.org/10.1002/2017JA025079)
- 592 Sarris, E. T., Krimigis, S. M., & Armstrong, T. P. (1976). Observations of  
593 magnetospheric bursts of high-energy protons and electrons at  $\sim 35 R_E$   
594 with Imp 7. *Journal of Geophysical Research*, *81*(13), 2341-2355. doi:  
595 <https://doi.org/10.1029/JA081i013p02341>
- 596 Sarris, E. T., Krimigis, S. M., Iijima, T., Bostrom, C. O., & Armstrong, T. P.  
597 (1976). Location of the source of magnetospheric energetic particle bursts  
598 by multispacecraft observations. *Geophysical Research Letters*, *3*(8), 437-440.  
599 doi: <https://doi.org/10.1029/GL003i008p00437>
- 600 Schindler, K. (1974). A theory of the substorm mechanism. *J. Geophys. Res.*, *79*,  
601 2803.
- 602 Scholer, M. (1984). Energetic ions and electrons and their acceleration processes  
603 in the magnetotail. In E. W. Hones, Jr. (Ed.), *Magnetic reconnection in space*  
604 *and laboratory plasmas* (p. 216). Am. Geophys. Union.
- 605 Scholer, M., Gloeckler, G., Hovestadt, D., Ipavich, F. M., Klecker, B., & Fan, C. Y.

- 606 (1983). Anisotropies and flows of suprathermal particles in the distant magne-  
 607 totail: ISEE 3 observations. *Geophysical Research Letters*, *10*(12), 1203-1206.  
 608 doi: <https://doi.org/10.1029/GL010i012p01203>
- 609 Scholer, M., Gloeckler, G., Hovestadt, D., Klecker, B., & Ipavich, F. M. (1984).  
 610 Characteristics of plasmoidlike structures in the distant magnetotail. *Jour-*  
 611 *nal of Geophysical Research: Space Physics*, *89*(A10), 8872-8876. doi:  
 612 <https://doi.org/10.1029/JA089iA10p08872>
- 613 Scholer, M., Gloeckler, G., Klecker, B., Ipavich, F. M., Hovestadt, D., & Smith,  
 614 E. J. (1984). Fast moving plasma structures in the distant magnetotail.  
 615 *Journal of Geophysical Research: Space Physics*, *89*(A8), 6717-6727. doi:  
 616 <https://doi.org/10.1029/JA089iA08p06717>
- 617 Scholer, M., & Jamitzky, F. (1987). Particle orbits during the development of plas-  
 618 moids. *J. Geophys. Res.*, *92*, 12,181.
- 619 Scholer, M., & Jamitzky, F. (1989). Plasmoid-associated energetic ion bursts in  
 620 the deep magnetotail: Numerical modeling of the boundary layer. *J. Geophys.*  
 621 *Res.*, *94*, 2459.
- 622 Sergeev, V. A., Pellinen, R. J., & Pulkkinen, T. I. (1996). Steady magnetospheric  
 623 convection: A review of recent results. *Space Sci. Rev.*, *75*, 551-604.
- 624 Slavin, J. A., Fairfield, D. H., Kuznetsova, M. M., Owen, C. J., Lepping, R. P.,  
 625 Taguchi, S., ... Reeves, G. D. (1998). ISTP observations of plasmoid ejection:  
 626 IMP 8 and Geotail. *Journal of Geophysical Research: Space Physics*, *103*(A1),  
 627 119-133. doi: <https://doi.org/10.1029/97JA02136>
- 628 Slavin, J. A., Hesse, M., Owen, C. J., Taguchi, S., Fairfield, D. H., Lepping, R. P.,  
 629 ... Sutcliffe, P. R. (1999). Dual spacecraft observations of lobe magnetic field  
 630 perturbations before, during and after plasmoid release. *Geophysical Research*  
 631 *Letters*, *26*(19), 2897-2900. doi: <https://doi.org/10.1029/1999GL003606>
- 632 Slavin, J. A., Lepping, R. P., Gjerloev, J., Fairfield, D. H., Hesse, M., Owen, C. J.,  
 633 ... Mukai, T. (2003). Geotail observations of magnetic flux ropes in the  
 634 plasma sheet. *Journal of Geophysical Research: Space Physics*, *108*(A1), SMP  
 635 10-1-SMP 10-18. doi: <https://doi.org/10.1029/2002JA009557>
- 636 Slavin, J. A., Tsurutani, B. T., Smith, E. J., Jones, D. E., & Sibeck, D. G. (1983).  
 637 Average configuration of the distant ( $<220 R_E$ ) magnetotail: Initial ISEE-3  
 638 magnetic field results. *Geophysical Research Letters*, *10*(10), 973-976. doi:  
 639 <https://doi.org/10.1029/GL010i010p00973>
- 640 Sun, W. J., Slavin, J. A., Tian, A. M., Bai, S. C., Poh, G. K., Akhavan-Tafti, M.,  
 641 ... Burch, J. L. (2019). MMS study of the structure of ion-scale flux ropes  
 642 in the Earth's cross-tail current sheet. *Geophysical Research Letters*, *46*(12),  
 643 6168-6177. doi: <https://doi.org/10.1029/2019GL083301>
- 644 Tsurutani, B. T., Slavin, J. A., Smith, E. J., Okida, R., & Jones, D. E. (1984). Mag-  
 645 netic structure of the distant geotail from -60 to -220  $R_e$ : ISEE-3. *Geophysical*  
 646 *Research Letters*, *11*(1), 1-4. doi: <https://doi.org/10.1029/GL011i001p00001>
- 647 Tsurutani, B. T., & von Rosenvinge, T. T. (1984). ISEE-3 distant geotail results.  
 648 *Geophysical Research Letters*, *11*(10), 1027-1029. doi: <https://doi.org/10.1029/GL011i010p01027>
- 649 Tsyganenko, N. (1987). Global quantitative models of the geomagnetic field in the  
 650 cislunar magnetosphere for different disturbance levels. *Planet. Space Sci.*, *35*,  
 651 1347-1358.
- 652 Vasyliunas, V. (1968). Observations of low-energy electrons in the evening sector of  
 653 the magnetosphere with OGO-1 and OGO-3. *J. Geophys. Res.*, *73*, 2839.
- 654 Zeleny, L., Lipatov, A., Lominadze, D., & Taktakishvili, A. (1984). The dynamics  
 655 of the energetic proton bursts in the course of the magnetic field topology re-  
 656 construction in the earths magnetotail. *Planetary and Space Science*, *32*(3),  
 657 313-324. doi: [https://doi.org/10.1016/0032-0633\(84\)90167-3](https://doi.org/10.1016/0032-0633(84)90167-3)
- 658 Zelenyi, L. M., Lominadze, J. G., & Taktakishvili, A. L. (1990). Generation of  
 659 the energetic proton and electron bursts in planetary magnetotails. *Jour-*  
 660

- 661 *nal of Geophysical Research: Space Physics*, 95(A4), 3883-3891. doi:  
662 <https://doi.org/10.1029/JA095iA04p03883>
- 663 Zhong, Z., Zhou, M., Burch, J., Tang, R., Deng, X., Turner, D., . . . Khotyaintsev,  
664 Y. (2020). Direct evidence for electron acceleration within ionscale flux rope.  
665 *Geophysical Research Letters*, 47(1).
- 666 Zwickl, R. D., Baker, D. N., Bame, S. J., Feldman, W. C., Gosling, J. T., Hones Jr.,  
667 E. W., . . . Slavin, J. A. (1984). Evolution of the earth's distant magne-  
668 totail: ISEE 3 electron plasma results. *Journal of Geophysical Research:*  
669 *Space Physics*, 89(A12), 11007-11012. doi: [https://doi.org/10.1029/](https://doi.org/10.1029/JA089iA12p11007)  
670 [JA089iA12p11007](https://doi.org/10.1029/JA089iA12p11007)

